Math Geosci
DOI 10.1007/s11004-014-9522-5

SPECIAL ISSUE

Analysis of Water Injection in Fractured Reservoirs Using a Fractional-Derivative-Based Mass and Heat Transfer Model

Anna Suzuki · Yuichi Niibori · Sergei A. Fomin · Vladimir A. Chugunov · Toshiyuki Hashida

Received: 9 July 2013 / Accepted: 10 January 2014

Abstract This research proposes a numerical scheme for evaluating the effect of cold-water injection into a geothermal reservoir. A fractional heat transfer equation (fHTE) is derived based on the fractional advection–dispersion equation (fADE) that describes non-Fickian dispersion in a fractured reservoir. Numerical simulations are conducted to examine the applicability of the fADE and the fHTE in interpreting tracer and thermal responses in a fault-related subsidiary structure associated with fractal geometry. A double-peak is exhibited when the surrounding rocks have a constant permeability. On the other hand, the peak in the tracer response gradually decreases when the permeability varies with distance from the fault zone according to a power law, which can be described by the fADE. The temperature decline is more gradual when the permeability of surrounding rocks varies spatially than when they have a constant permeability. The fHTE demonstrates good agreement with the temperature profiles for the different permeabilities of surrounding rocks. The retardation parameters in the fADE and the fHTE increase with the permeability of the surrounding rocks. The orders of the temporal fractional derivatives in the fADE and the fHTE vary with the permeability patterns.

A. Suzuki (✉)
Graduate School of Environmental Studies, Tohoku University, 6-6-11-707, Aramaki Aza Aoba, Aoba, Sendai, Miyagi 980-8579, Japan
e-mail: anna.suzuki@rift.mech.tohoku.ac.jp

Y. Niibori · T. Hashida
Graduate School of Engineering, Tohoku University, Sendai 980-8579, Japan

S. A. Fomin
Department of Mathematics and Statistics, California State University, Chico, CA 95929, USA

V. A. Chugunov
Department of Applied Mathematics, Kazan Federal University, Kazan 420008, Russia

Published online: 18 February 2014

Keywords Geothermal reservoir · Tracer test · Thermal breakthrough · Fractional advection–dispersion equation · Fault zone

1 Introduction

The lifespan of geothermal resources can be extended through reinjection, which prevents a decline in pressure as well as the exhaustion of water in a geothermal reservoir. One of the major problems with this process, however, is the possibility of an early thermal breakthrough in the production well. This premature breakthrough, together with injection-induced cooling, continues to pose a challenge to injection into geothermal reservoirs.

Tracer testing is a standard method for tracing mass transport inside a geothermal reservoir, and is a valuable tool in the design and management of production and injection operations. The advection–dispersion equation (ADE) based on Fick's law has been widely used to solve a range of problems in the analysis of tracer transport. The Fickian solution, however, produces conflicts in highly fractured reservoirs where the heavy tailing of tracer breakthrough is often observed. To model the non-Fickian behaviors obtained from fractured reservoirs, several tracer transport models have been proposed. For example, the dual-porosity model has been developed to extend the ADE, which simulates solute transport due to the presence of high-permeability and low-permeability domains (Coats and Smith 1964). In a fractured geothermal reservoir, the multiple flow-path model has been used frequently (Horne 1981; Axelsson et al. 2001); this model is composed of several flow paths that may be isolated from one another by fracture distributions.

The concept of fractional derivatives has recently been used to develop a mass transport model, resulting in the fractional advection–dispersion equation (fADE) (Benson et al. 2000). Using fractional derivatives in time and space, Fomin et al. (2005) derived an equation that accounts for the diffusion of a solute into the surrounding rock through fractal geometry. This model enables a reproduction of the tracer responses, including the heavy tails, observed in geothermal fields.

At the field scale, Massart et al. (2010) indicated that the fault and fracture networks control global permeability in geothermal reservoirs, based on statistical characterization of the fractures. In addition, secondary fractures associated with larger faults, referred to as the damage zone, appear in geothermal reservoirs. Fluid flow between injection and production wells is obviously subject to the influence of structure of the fault and of the surrounding damage zone; thus, the understanding of this influence is fundamental for solving reinjection problems in a geothermal field. Savage and Brodsky (2011) suggested that the fracture density decays with distance from isolated faults according to a power law in the outer damage zone of the faults. The assumption of the fADE is that the diffusivity varies with the distance from the reservoir according to a power law. Hence, the fADE is expected to offer a realistic interpretation of mass transport in the rocks surrounding the fault zone.

Other methods of evaluating aspects of reinjection using tracer response curves have been studied previously. The chemical front is closest to the thermal front with regard to its transport properties and can be used as a precursor of thermal breakthrough

because it arrives earlier. Migration of the cold-water front for a single-phase liquid flow that conducts heat from a semi-infinite matrix is fairly well understood through the work of Lauwerier (1955) and Bodvarsson (1972). Consequently, the changes in temperature with time at the production wells have been estimated (Gringarten and Sauty 1975; Bodvarsson and Tsang 1982; Kocabas 2004). This model has been widely used to estimate the cooling effects of the reinjected fluid in several geothermal fields, but leads to an overestimation of temperature decline (Aksoy et al. 2008). Shook (2001) proposed tracer analysis methods that predicted thermal breakthrough in geothermal reservoirs. This study indicated that transforming the variables of the tracer data provides a quick and simple means of predicting the beginning of cooling of the produced fluids under the assumption that heat conduction is negligible. As transverse heat conduction may occur and play an important role in temperature change in fractured reservoirs, this study also pointed out that modifications to the method are required to extend it to fractured media.

Over the last decade, many authors have made notable contributions to both the theory and application of the fADE in hydrology, as reviewed by Zhang et al. (2007). The advantage of using fADE is its ability to describe fluid flow in a geothermal field with large spatial and temporal heterogeneities based on a mathematical description of the fractal geometry (Fomin et al. 2011). Suzuki et al. (2012) demonstrated that the fADE offers a method for predicting tracer responses irrespective of differing well intervals in a fractured reservoir. Further research on the application of the fADE should be performed to evaluate and optimize geothermal development. A fractal model for the heat transfer of nanofluids has been introduced and the relationship to mass transport has been investigated (Xiao et al. 2009); however, very few attempts have been made to combine the fADE and any heat transfer process. As the fADE can be used to describe the mass transport interaction between a reservoir and the surrounding formation, it is reasonable to suppose that the effect of heat transfer into the surrounding rocks could be described by extension of the fADE.

This paper proposes a new heat transfer equation based on fractional derivatives by developing the fADE. This study focuses on the effects of diffusion and heat transfer into the surrounding rocks of a fault zone on tracer and thermal responses. For simplicity, synthetic field performance data are generated using the TOUGH2 reservoir simulator, and then used to demonstrate the applicability of the fADE and the proposed heat transfer model.

The following section introduces the proposed mathematical heat transfer model. Section 3 describes the numerical methods that generate synthetic field performance data and analyzes the data by the fADE and the heat transfer model. Section 4 discusses the results obtained from the fADE and the heat transfer model, and compares the models with the results obtained from the TOUGH2 reservoir simulator. Finally, the conclusions of this study are given in Sect. 5.

2 Mathematical Model

A schematic of a fractured reservoir is illustrated in Fig. 1. Massart et al. (2010) suggested that bulk permeability in a geothermal reservoir is dominated by a large-

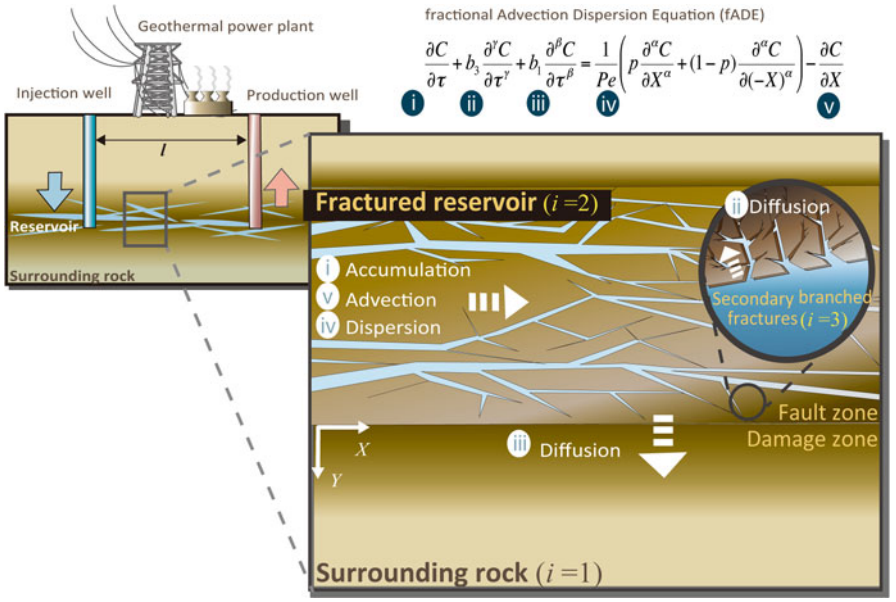

Fig. 1 Schematic of a reservoir

scale fault that forms the main conduit of fluid flow. In the present study, the fractured reservoir is assumed to consist of a highly permeable fault zone. The reservoir is surrounded by impermeable rocks, and the rock matrix inside the reservoir consists of porous media. The indices of the physical properties, $i = 1$, 2, and 3, denote the surrounding rocks, the fractured reservoir (fault zone), and the porous blocks, respectively. Cartesian coordinates (x, y) are chosen in such a manner that fluid in the reservoir flows in the x direction and the y axis is perpendicular to the fluid flow. The interface between the fault zone and the surrounding rock lies at $y = 0$.

The fADE can be expressed as follows (Fomin et al. 2005, 2011)

$$\frac{\partial C}{\partial \tau}+b_3\frac{\partial C}{\partial \tau}+b_1\frac{\partial C}{\partial \tau}=\frac{1}{Pe}\left(p\frac{\partial^\alpha C}{\partial X^\alpha}+(1-p)\frac{\partial^\alpha C}{\partial(-X)^\alpha}\right)-\frac{\partial C}{\partial X}, \qquad (1)$$

where τ is time, X is distance from the injection zone, and C is the tracer concentration in the reservoir. The coefficients b_3 and b_1 represent retardation processes caused by the diffusivities into the secondary branched fractures and into the surrounding rocks, respectively. Pe is the Peclet number, the orders β $(0 < \beta \leq 1)$ and γ $(0.5 \leq \gamma \leq 1)$ are the orders of the fractional temporal derivatives, α $(0 < \alpha \leq 1)$ is the order of the fractional spatial derivative, and p $(0 \leq p \leq 1)$ is the skewed parameter that controls the bias of the dispersion (Huang et al. 2008). The first term of the left-hand side is an accumulation term and the second term of the left-hand side expresses the diffusion into secondary branched fractures. The third term of the left-hand side represents the diffusion into the surrounding rocks. The right-hand side includes dispersive and advective terms. Equation (1) has been non-dimensionalized using characteristic scales (Suzuki et al. 2012).

The aim of the present study is to propose a new heat transfer model to characterize the thermal response in a fractured reservoir based on the fADE. This study limits the discussion to the effects of the diffusion into the surrounding rocks in the derivation of the heat transfer model. A damage zone of subsidiary structures that surround the fault zone which are mechanically related to the growth of the fault zone has been observed (Evans et al. 1997; Le Garzic et al. 2011). Savage and Brodsky (2011) suggested that the fracture density FD at the damage zone decays with distance from faults according to a power law as follows

$$\mathrm{FD} = \mathrm{FD}_0 r^{-n}, \tag{2}$$

where FD_0 is the fault constant (the fracture density at 1 m from the fault), r is the distance from the fault, and n is the exponent describing the decay. Since fracture structures affect permeability, consideration of the fault-related subsidiary structure may provide knowledge for permeability evaluation of a reservoir.

A fractal diffusion equation based on fractal geometry, in which the diffusion coefficient decreases with distance according to a power law, can be converted into a term of a temporal fractional derivative (Samko et al. 1993; Fomin et al. 2011). This is depicted as the third term of the left-hand side of Eq. (1). Detailed derivations of the term can be found in the literature (Fomin et al. 2005, 2011). Analogous behaviors of heat and mass transfer have been long recognized (Welty et al. 2007). Thus, the heat conduction equation may also be expressed using a heat conduction coefficient that decreases with distance according to a power law as follows

$$\frac{\partial T}{\partial t} = \frac{\partial}{\partial y}\left(\lambda_1 y^{-\eta'} \frac{\partial T}{\partial y}\right), \tag{3}$$

where t is the time, y is the distance from the reservoir, T is the temperature of the surrounding rocks, λ_1 is the thermal conductivity of the surrounding rocks, and η' is an exponent describing the decay of temperature in the surrounding rocks.

Thermal conduction in the reservoir is assumed to be negligible, as indicated by Woods and Fitzgerald (1993). The heat transfer equation including the effect of heat transfer into the surrounding rocks can be written as

$$\overline{\rho C_{\mathrm{p2}}} \frac{\partial T_2}{\partial t} + d_1 \frac{\partial^{\beta'} T_2}{\partial t^{\beta'}} = -m_2 \rho_{\mathrm{w}} C_{\mathrm{pw}} v \frac{\partial T_2}{\partial X}, \tag{4}$$

where $\overline{\rho C_{\mathrm{p2}}} = m_2 \rho_{\mathrm{w}} C_{\mathrm{pw}} + (1 - m_2) \rho_{\mathrm{r}} C_{\mathrm{p2}}$; ρ_{w} and ρ_{r} are the density of water and rock, respectively; $\mathrm{C_{pw2}}$ and $\mathrm{C_{pr2}}$ are the heat capacity of water and rock in the reservoir, respectively. t is the time, x is the distance from the injection zone, T_2 is the temperature of the reservoir, m_2 is the porosity of the reservoir, and v is the fluid velocity. The coefficient of the second term on the left-hand side is set to d_1, which denotes the retardation factor associated with heat loss from the surrounding rocks. The order β' ($0 < \beta' \leq 1$) is the order of the fractional derivatives with respect to time. The scale of heat transfer time t_{h} represents the characteristic time of the heat migration over

the well spacing l. The non-dimensional variables that non-dimensionalize Eq. (4) are the following

$$\tau = \frac{t}{t_{\mathrm{h}}}; \quad X = \frac{x}{l}; \quad \mathrm{T} = \frac{T_2}{T_m}; \quad e_1 = \frac{d_1}{\overline{\rho C_{\mathrm{p}}} t_{\mathrm{h}}^{\beta'-1}}, \tag{5}$$

where T_m is the representative temperature.

Since this study focuses on the effect of diffusion into the surrounding rocks, transport processes due to diffusion into secondary branched fractures and dispersion in a fault zone, which are described by the second term on the left-hand side and the first and the second terms on the right-hand side of Eq. (1), are neglected. The mass and heat transfer equations used in this study are described as follows

$$\frac{\partial C}{\partial \tau} + b_1 \frac{\partial^{\beta} C}{\partial \tau^{\beta}} = -\frac{\partial C}{\partial X} \quad \text{and} \tag{6}$$

$$\frac{\partial \mathrm{T}}{\partial \tau_h} + e_1 \frac{\partial^{\beta'} \mathrm{T}}{\partial \tau_h^{\beta'}} = -\frac{\partial \mathrm{T}}{\partial X}. \tag{7}$$

Hereafter, the Eqs. (6) and (7) are referred to as the fADE and the fractional heat transfer equation (fHTE).

3 Numerical Simulation Methods

3.1 Problem Setup for Generation of Synthetic Data

The influence of injected water on tracer and thermal responses for different permeability distributions of the surrounding rocks is investigated using the general-purpose reservoir simulator TOUGH2 (Pruess et al. 1999). In this study, the synthetic data generated by TOUGH2 are regarded as data obtained in the field to illustrate the applicability of the fADE [Eq. (6)] and the fHTE [Eq. (7)]. Fluid, mass, and heat flow are numerically simulated in a reservoir model. The reservoir consists of a fault zone with high permeability, which is surrounded by impermeable rocks. Figure 2 shows a schematic of the numerical simulation model. The numerical properties are summarized in Table 1. The thickness T and length L of the calculation domain are set to $T = 20$ m and $L = 80$ m, respectively. The X-axis is the median line of the fault zone ($Y = 0$ m). The simulation domain is discretized by 80×18 grid blocks. The cell sizes are refined in the proximity of the interface between the fault zone and the surrounding rocks. The cell sizes are set to 1 m $\times$ 1 m $\times$ 1 m, except for the refined cells where the cell sizes are set to 1 m $\times$ 0.1 m $\times$ 1 m.

This study discusses the structure of the surrounding rocks of a fault zone and the transport behaviors due to the structure. Therefore, the simulation program is set up to be as simple as possible to focus only on the permeability of the surrounding rocks. The flow domain is assumed to be homogeneous for a permeability of 1×10^{-13} m^2. A no-flow condition is applied on the lateral boundary. Dirichlet conditions

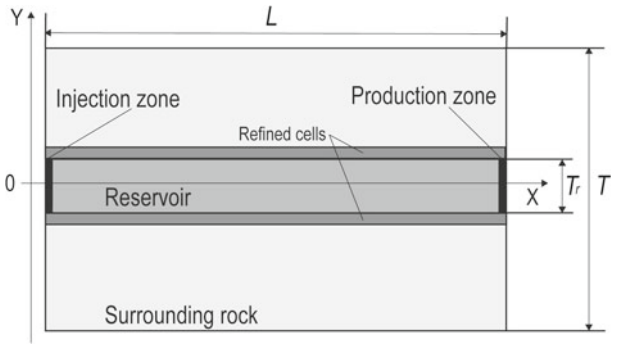

Fig. 2 Simulation model to evaluate the effects of cold-water injection. The reservoir size parameters L, T, and T_r are set to 80, 20, and 2 m, respectively

Table 1 Summary of the reservoir and numerical properties

Property	
Calculation domain	
Thickness T	20 m
Length L	80 m
Thickness of reservoir T_r	2 m
Permeabilities	
Reservoir	1.0×10^{-13} m^2
Surrounding rock	$0-1 \times 10^{-14}$ m^2
Porosity	0.1
Rock density	2,600 kg/m^3
Rock heat capacity	1 kJ/kg °C
Thermal conductivity	0 W/m °C
Initial pressure	10 MPa
Initial temperature	175 °C
Injection rate	0.2 kg/s
Injection temperature	35 °C
Productivity Index	1×10^{-8} m^3
Production pressure	9 MPa

can be implemented on the grid blocks adjacent to the top and bottom boundaries. The injection takes place along the left side of the domain ($X = 0$ m), and the extraction is performed on the right side ($X = 80$ m). One-dimensional bulk flow occurs from the inlet toward the outlet, and advective transport is dominant in the flow domain. The tracer is injected at 0.2 kg/s for one day, after which the injection is switched to fresh water. Provided that the rock grains are sufficiently small and the fluid velocities are sufficiently low, local thermodynamic equilibrium between the rock and fluid can be assumed. It is also assumed that the rock is incompressible, that both rock and fluid have constant thermal properties, and that thermal conduction is neglected. Continuous cold-water injection is simulated until the thermodynamic state of the reservoir is in equilibrium.

To evaluate the influence of permeability distributions in the surrounding rocks, two models of surrounding rocks are used in this study: (1) the distribution of permeability is kept constant throughout domain and (2) the permeability of the surrounding rock, K_s, in such a case is defined as a function of a power law in the following form

$$K_s(y) = K_r \left(y - \frac{T_r}{2} \right)^{-\theta}, \tag{8}$$

where K_r is the constant permeability of the reservoir, T_r is the thickness of the reservoir, y is the distance form the reservoir and θ is the index of anomalous dispersion. The latter is based on the decay of the fracture density with distance from the fault zone (Savage and Brodsky 2011).

3.2 Numerical Procedure for Solving Fractional-Derivative Equations

To analyze tracer breakthroughs and temperature histories using the fADE and the fHTE, a finite difference approach for solving Eqs. (6) and (7) is hereby presented.

It is assumed that $0 \leq C(X, \tau)$ over the region $0 \leq X \leq L$, $0 \leq \tau \leq \tau_{\max}$. In addition, $\tau_n = n\Delta\tau$ is defined as the integration time ($0 \leq \tau_n \leq \tau_{\max}$) and $\Delta X > 0$ is the grid size in the spatial dimension, where $\Delta X = L/NX$ and $X_i = i\Delta X$ for $i = 0, \ldots, NX$. Consider an approximation to $C(X_i, \tau_n)$. The finite difference solution is obtained by combining Eqs. (6) and (7), which are discretized in time using an implicit (Euler) method as follows

$$\frac{C_i^{n+1} - C_i^n}{\Delta T} + \frac{b_1}{\Delta T^{\beta}} \sum_{k=0}^{n} w_k^{n-k+1} = \frac{C_i^{n+1} - C_{i-1}^{n+1}}{\Delta X} \quad \text{and} \tag{9}$$

$$\frac{\mathrm{T}_i^{n+1} - \mathrm{T}_i^n}{\Delta T} + \frac{e_1}{\Delta T^{\beta'}} \sum_{k=0}^{n} w_k^{n-k+1} = \frac{\mathrm{T}_i^{n+1} - \mathrm{T}_{i-1}^{n+1}}{\Delta X}, \tag{10}$$

where

$$w_0^{\beta} = w_0^{\beta'} = 0, \quad w_k^{\beta} = (-1)^k \frac{(\beta+1)\beta(\beta-1)\ldots(\beta-k+1)}{k!},$$
$$w_k^{\beta'} = (-1)^k \frac{(\beta'+1)\beta'(\beta'-1)\ldots(\beta'-k+1)}{k!},$$

ΔX is the grid size and ΔT is the integration time. The term X_i is used to represent the coordinate of the ith grid and C_i^n is the concentration of the ith grid at the nth time step.

3.3 Fitting Procedure

The tracer responses and thermal responses calculated using TOUGH2 are normalized via representative physical variables: the representative distance l is the well spacing

(80 m). The representative time τ is the average travel time, which is calculated from the first peak of tracer concentration and depicts the mean advective time of the system. The concentration C is expressed as the mass fraction of tracer produced at the outlet. The tracer recovery rate is calculated using tracer responses. The normalized temperature, $T[-]$, is expressed as

$$\mathrm{T}[-] = \frac{T_{\mathrm{pro}}(t) - T_{\mathrm{in}}}{T_{\mathrm{r}} - T_{\mathrm{in}}}, \tag{11}$$

where T_{pro} is the temperature of fluid produced at the outlet, T_{r} is the initial temperature of the reservoir, and T_{in} is the temperature of injected water.

Flow simulation with TOUGH2 is performed without considering solute diffusion and heat conduction. Since fluid flow in the flow domain is dominated by the advective process, the first and second terms of the right-hand side in Eq. (7) are negligible. The parameters required to fit the tracer data calculated by TOUGH2 are b_1 and β, which are obtained from the root-mean-square error (RMSE)

$$\mathrm{RMSE} = \sqrt{\frac{1}{N}\sum_{i=1}^{N}\left(C_i^{\mathrm{fADE}} - C_i^{\mathrm{tracer}}\right)^2}, \tag{12}$$

where N is the number of data points, C_i^{fADE} is the ith concentration calculated using the fADE, and C_i^{trace} is the ith concentration obtained using TOUGH2. The parameters e_1 and β' in Eq. (7) are also determined in the same manner.

4 Results and Discussion

4.1 Properties of the fADE and the fHTE

The effects of β and b_1 on tracer response are shown in Fig. 3. Figure 3a shows tracer responses when β is equal to 1 in the fADE. The tracer responses lead to symmetric Gaussian curves. On the other hand, when b_1 is equal to 1 and β is smaller than 1, the peak concentration tends to decrease with a smaller β, and the response curve exhibits a heavy tail (Fig. 3b). A smaller value for β indicates that greater volumes of tracer are diffusing into the surrounding rocks and leads to a heavier tailing of the tracer response.

The effects of β' and e_1 on thermal response are shown in Fig. 4. The initial temperature of the reservoir, T_{r}, and the injection temperature, T_{in}, of the water are set to $T_{\mathrm{r}}[-] = 1$, $T_{\mathrm{in}}[-] = 0$, respectively. Figure 4a shows the temperature profiles when β' is equal to 1 in the fHTE. In this case, there is a sharp decrease in temperature following breakthrough. A higher value of e_1 results in delayed breakthrough. On the other hand, the change in β' for $e_1 = 1$ produces different slopes in the temperature decline curves (Fig. 4b). The production temperature for $\beta' = 1$ drops to T_{in}, while the production temperature for the smaller β' does not decrease to T_{in}. The β' value may allow us to predict the achieving temperature due to cold-water injection. If the β value is related to the β' value, β is capable of estimating the β' value.

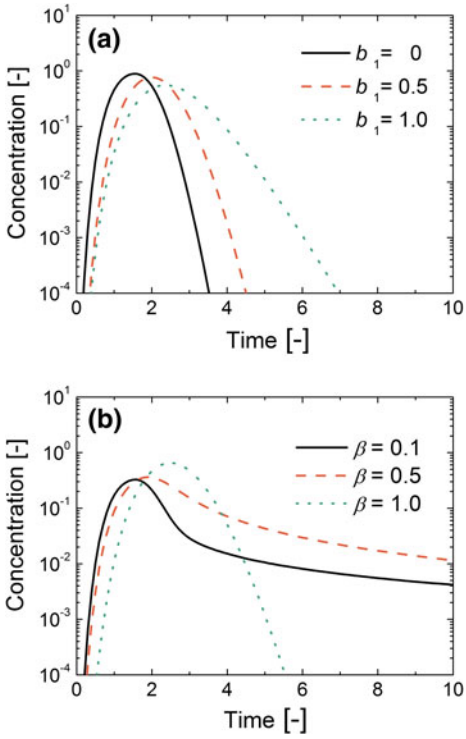

Fig. 3 Tracer responses calculated for various values of b_1 and β

4.2 Simulation Results of TOUGH2

The effect of water injection on reservoir performance is examined using TOUGH2. The influence of permeability distributions in the surrounding rocks is shown in Figs. 5 and 6. Figure 5 shows tracer responses when the permeability of the surrounding rocks, K_s, is constant. Constant values of K_s between 0 and 1×10^{-14} m^2 are used. When K_s is equal to 0, the tracer response is a symmetric Gaussian distribution. This is because the tracer transport process is governed solely by advection. For the case when K_s is greater than 0, the tracer response exhibits apparently a long tail and a second peak. The double-peak responses indicate that there are two distinct flow pathways between wells. If a fault zone is surrounded by permeable rocks, then mass exchange between the fault zone and the surrounding rocks occurs. In this case, the tracers will travel not only inside the fault zone, but also through the surrounding rocks. Thus, the first peak in the tracer response is produced by advective flow in the reservoir, and the second peak is then produced as a result of diffusion into the surrounding rocks.

Figure 8 shows the effect of permeability distribution in the surrounding rocks on tracer response. For a spatially varying permeability distribution in the surrounding rocks, the permeability is defined according to a power law as in Eq. (8). The permeability of the reservoir is $K_r = 1 \times 10^{-13}$ and the index of anomalous dispersion θ ranges 1.5–2.5. The results of a spatially varying permeability for $\theta = 1.8$ and a constant permeability for $K_s = 3 \times 10^{-15}$ are plotted. It is worth noting that in

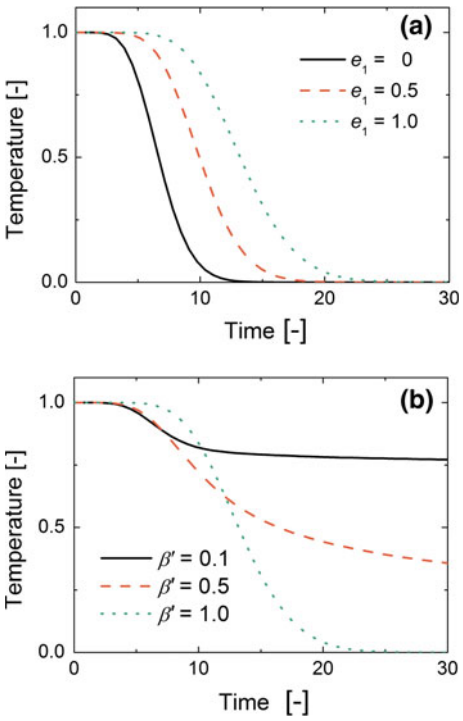

Fig. 4 Temperature profiles computed for various values of e_1 and β'

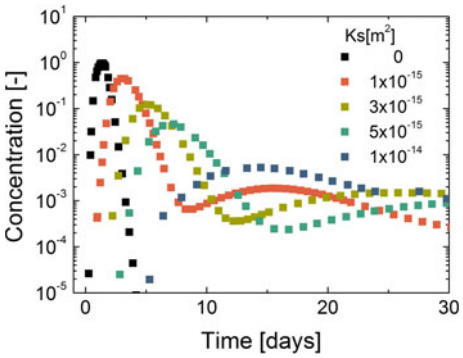

Fig. 5 Tracer responses calculated by TOUGH2 for various values of constant permeability of the surrounding rocks

both cases, the permeabilities of the top and bottom boundaries of the calculation domains are of the same value. Compared to the constant permeability distribution of the surrounding rocks, the spatially varying distribution produces a retardation in the arrival time of the tracer peak and a decrease in the peak concentration. In addition, an apparent second peak is not observed for the case of spatially varying permeability. In this case, the flow domains are not distinguished as merely two domains. Several flow patterns are considered to occur due to the wide range of permeabilities of the surrounding rocks, and the superposition of the tracer responses for each pattern may produce a gradual decrease in the concentration profile.

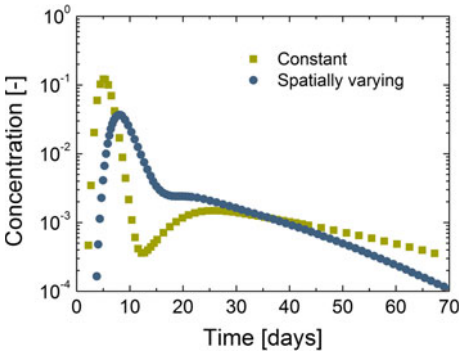

Fig. 6 Effects of different permeability distributions on tracer response: a constant permeability of $K_s = 3 \times 10^{-15}$ and a spatially varying permeability of $\theta = 1.5$

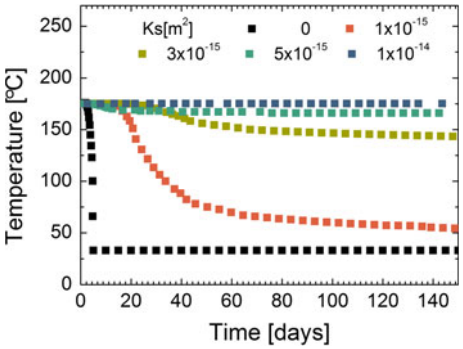

Fig. 7 Temperature histories for various values of constant permeability of the surrounding rocks

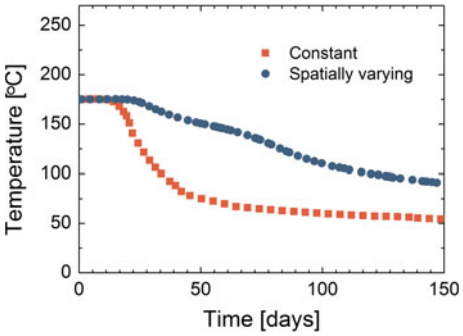

Fig. 8 Effects of different permeability distributions on temperature decline for a constant permeability of $K_s = 1 \times 10^{-15}$ and for a spatially varying permeability of $\theta = 2$

Temperature profiles for different permeability distributions in the surrounding rocks are shown in Figs. 7 and 8. The initial temperature of the reservoir, T_r, is set to 175 °C, and the temperature of the injected water, T_{in}, is set to 35 °C. The calculated temperature using TOUGH2 achieves a state of thermodynamic equilibrium after a significant time (100 years) denoted by T_e. Figure 7 shows temperature profiles when the permeability of the surrounding rocks, K_s, is constant. When K_s is equal to 0, there is a rapid thermal breakthrough and the temperature drops to T_{in}. On the other hand, the temperature does not reach T_{in} for the case when K_s is greater than

0. Note that the heat conduction is neglected in TOUGH2 for simplicity. Thus, the temperature change is subject to fluid flow. Since a tracer response for the case of constant permeability is divided into two processes, in an analogous way, the heat transfer can be also divided into two phases. First, temperature drops rapidly due to fluid flow in the fault zone, and then the change in temperature occurs slightly according to the diffusion into surrounding rocks. Figure 8 shows the effect of permeability distribution in the surrounding rocks on temperature profile. The results of a spatially varying permeability for $\theta = 2$ and a constant permeability for $K_s = 1 \times 10^{-15}$ are plotted. In both cases, the permeabilities of the top and bottom boundaries of the calculation domains are 1×10^{-15} m^2. A rapid temperature decline is observed in the case of constant permeability, compared with a temperature profile for the case of spatially varying permeability. Recall that a spatially varying permeability distribution in the surrounding rocks results in a gradual mass exchange into the surrounding rocks. Therefore, it is suggested that the spatially varying permeability distribution leads to a gradual heat exchange with the surrounding rocks, as shown in Fig. 8.

The equilibrium temperature T_e and the recovery rate f for the cases of constant and spatially varying permeabilities are presented in Tables 2 and 3, respectively. When K_s is equal to 0, f is found to be 1. In this case, T_e has the same value as T_{in}. This

Table 2 Characteristics of tracer and thermal responses and estimated parameters of the fADE, ADE, and fHTE for a constant permeability of the surrounding rocks

K_s (m^2)	f	T_e (°C)	ADE	fADE		fHTE	
			b_1	b_1	β	e_1	β'
0	1.00	35	0.0	0.0	–	0.0	–
1×10^{-15}	0.90	46	0.0	0.04	0.1	0.9	0.4
2×10^{-15}	0.72	103	0.0	0.4	0.1	1.2	0.1
3×10^{-15}	0.54	136	0.0	0.6	0.1	2.0	0.1
5×10^{-15}	0.31	158	1.0	1.3	0.1	3.1	0.1
1×10^{-14}	0.15	170	10.0	2.5	0.1	5.0	0.1

Here, K_s is the constant permeability, f is the recovery rate, and T_e is the equilibrium temperature of the production area after a significant amount of time (100 years)

Table 3 Characteristics of tracer and thermal responses and estimated parameters of the fADE, ADE, and fHTE for a spatially varying permeability of the surrounding rocks

θ	K_b (m^2)	f	T_e (°C)	ADE	fADE		fHTE	
				b_1	b_1	β	e_1	β'
1.5	3×10^{-15}	0.25	157	0.7	1.5	0.1	2.9	0.1
1.8	2×10^{-15}	0.47	131	0.5	0.8	0.2	2.3	0.2
2	1×10^{-15}	0.86	68	0.2	0.3	0.3	1.9	0.5
2.5	4×10^{-16}	1.00	41	0.1	0	1.0	1.6	0.7

Here, $K_s(y) = y^{-\theta} \times 10^{-13}$, where K_s is the constant permeability; K_b is the permeability of the boundary of the calculation domain; f is the recovery rate; and T_e is the equilibrium temperature of the production area after a significant amount of time (100 years)

indicates that all injected tracer arrives at the production zone and all the injected water influences the cooling in the reservoir. In contrast, for the case of permeable surrounding rocks, T_e does not drop to T_{in} (Table 2). A higher permeability of the surrounding rocks leads to a lower recovery rate, resulting in a smaller temperature variation from T_r. Therefore, T_e has a highly negative correlation with f. To predict temperature of produced fluids, the recovery rate obtained from the tracer response is a significant parameter.

4.3 Application of Fractional-Derivative-Based Models

The concentration and temperature results obtained using TOUGH2 (Figs. 5, 6, 7, 8) are used to validate the applicability of the fADE and the fHTE. Figure 9 shows the best-fit curves of the fADE on plots of the calculated tracer responses. For comparison, the best-fit curves of the classical ADE are also plotted.

As mentioned previously, the calculated tracer response for $K_s = 0$ is expected to be Gaussian. Both the fADE and the ADE with $b_1 = 0$ can characterize the tracer response computed by TOUGH2 (Fig. 9a). Figure 9b shows the tracer response for a constant permeability of $K_s = 3 \times 10^{-15}$ along with the best-fit curves of the fADE and the ADE. It appears that the ADE solution provides no long tail and deviates significantly from the long-term tracer response. The fADE fitting result captures the overall trend of the tracer response and is well matched with the long-term behavior; however, this result shows disagreement with the double-peak behavior in the tracer response. This discrepancy is due to the derivation of the fADE and is derived based on fractal geometry (Fomin et al. 2011); thus, the fADE does not necessarily describe the detail of the double-peak behavior.

Figure 9c shows the best-fit curves of the fADE and the ADE for a spatially varying permeability distribution in the surrounding rocks. In this case, a permeability distribution computed by TOUGH2 follows the power law given in Eq. (8). On the other hand, the diffusion coefficient in the fADE has been defined to decrease with distance from the fault zone according to a power law(Fomin et al. 2005). Therefore, the fADE fitting result is in reasonable agreement with the calculated tracer response.

The fitting parameters, b_1 and β, for the cases of constant and spatially varying permeability are listed in Tables 2 and 3, respectively. It is likely that a higher value of K_s gives a higher b_1 for both permeability distributions. For the case of constant permeability of the surrounding rocks, β is independent of the value of permeability, whereas for the spatially varying case, β decreases with increasing permeability in the surrounding rocks. The parameters of the fADE are thought to correlate with the structure of the surrounding rocks. This correlation will be investigated in our future work.

The fADE can describe anomalous behaviors of tracer responses using few parameters. This study used two parameters, namely, b_1 and β. A general-purpose reservoir simulator, that is TOUGH2, embodies all of essential properties of a reservoir based on variable information such as geological, hydrological, and geochemistrical data. At the beginning of any field development or when extending the development field, available data from the field are limited and make it difficult to simulate a complex and

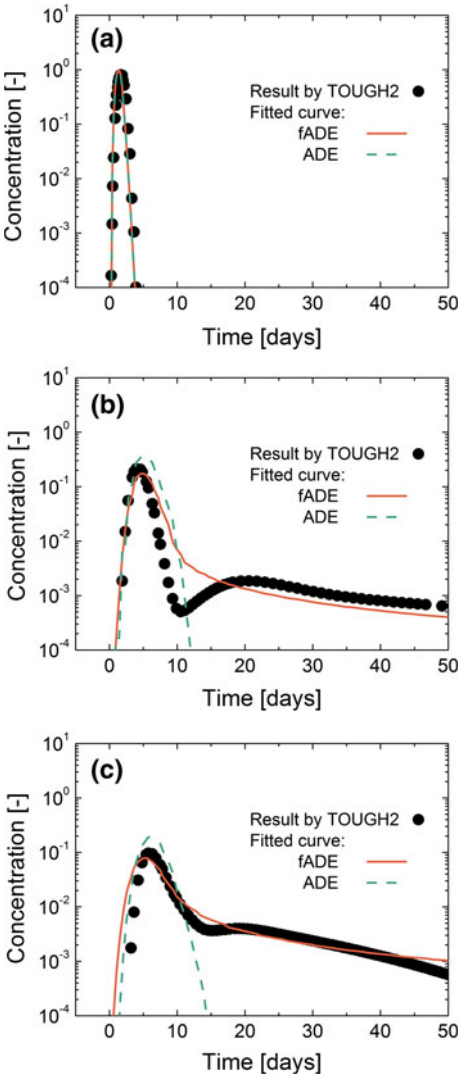

Fig. 9 Simulated tracer responses by TOUGH2 (*symbols*) (Figs. 5, 6) and best fits with the fADE (*solid lines*) and the ADE (*dashed lines*) for (**a**) $K_S = 0$, (**b**) constant permeability ($K_S = 1 \times 10^{-15}$), and (**c**) spatially varying permeability ($\theta = 1.5$)

heterogeneous reservoir. In addition, the limited information is incapable of providing unique model-constitutive parameters in the numerical simulation. In such cases, the fADE, which summarizes the complexity of fracture distribution based on fractal geometry, is expected to quickly and efficiently analyze mass transport in a fractured reservoir.

To verify the applicability of the fHTE, the equation is applied to the calculated temperature profiles. Figures 10 and 11 show the best-fit curves of the fHTE on the calculated temperature profiles. It appears that the solutions of the fHTE are in good agreement with the calculated temperature profiles for both cases of constant and spatially varying permeability. As mentioned before, it has been shown that the fADE does not express the double-peak feature of the tracer response for a constant perme-

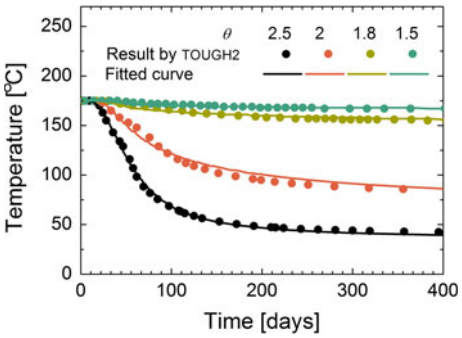

Fig. 10 Simulated temperature profiles using TOUGH2 for constant permeability (*squares*) (Fig. 7) and the fitting curve of the fHTE (*solid lines*)

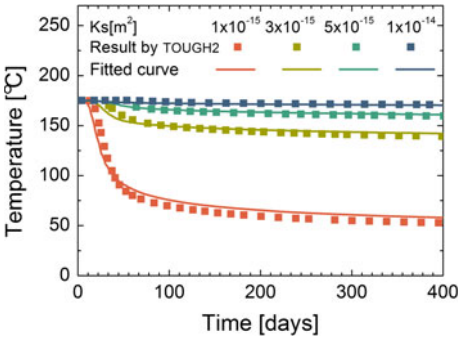

Fig. 11 Simulated temperature profiles using TOUGH2 for a spatially varying permeability (*squares*) and the fitting curve of the fHTE (*solid lines*)

ability (Fig. 9b). However, the temperature profiles (Fig. 10) can be well characterized by the fHTE. This is because thermal response has less sensitivity to water injection than the tracer response and is not subject to the strong influence of two distinct flow domains.

The fitting parameters of the fHTE, e_1 and β', are presented in Tables 2 and 3, respectively. For the case of constant permeability, the optimized values of β' in the fHTE are 0.1, which are the same values as for β in the fADE, except for $K_s = 1 \times 10^{-15}$ m^2. For $K_s = 1 \times 10^{-15}$ m^2, the value of b_1 is shown to be considerably small and the estimated values for β are taken to include a significant error. For the case of spatially varying permeability, β' decreases with an increase in a permeability of the surrounding rocks, and β' in the fHTE values is close to that of β in the fADE. For both permeability cases, a highly permeable surrounding rock leads to a higher e_1. This trend in e_1 is similar to that in b_1, which was obtained from the curve fitting of the tracer responses; however, e_1 is apparently greater than b_1. Further understanding of the relationship between the parameters should be useful for predicting premature thermal breakthrough based on a tracer response obtained from the field.

A comparison with other models proposed by previous studies is shown in Fig. 12. Figure 12a, b are temperature profiles for a constant permeability of $K_s = 1 \times 10^{-15}$ and for a spatially varying permeability of $\theta = 2$, respectively.

Lauwerier (1955) developed an analytical solution for the heat transfer during one-dimensional flow with heat loss. Gringarten and Sauty (1975) extended this approach to confining beds and reinjection problems in geothermal fields. Their heat loss model is the same as Eq. (7) for $\beta' = 1$, and the equivalent value of e_1 expresses the thermal

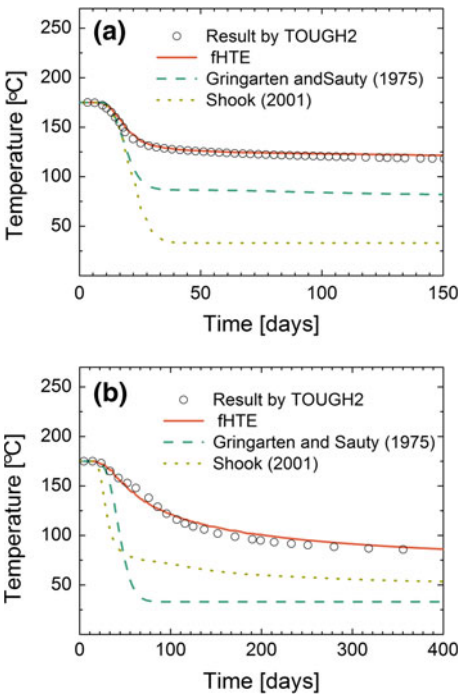

Fig. 12 Fitted curves of the heat loss model given by Gringarten and Sauty (1975) (*dashed lines*) and prediction results of the transformation method by Shook (2001) (*dotted lines*) on a temperature decline for **a** a constant permeability ($K_S = 1 \times 10^{-15}$) and **b** a spatially varying permeability ($\theta = 2$)

conductivity of cap rocks. The results suggest that the heat loss model (Gringarten and Sauty 1975) can describe the beginning of temperature decline for a constant permeability, which shows the comparatively rapid decrease (Fig. 12a). However, it shows disagreement with the temperature change in the case of spatially varying permeability of the surrounding rocks (Fig. 12b). In addition, in both permeability cases, there are apparent differences between T_e calculated by TOUGH2 and T_e estimated by the heat loss model.

Shook (2001) proposed a method for predicting thermal breakthrough using tracer histories, which are transformed through a simple variable transformation. Shook concluded that the method could work well for single-phase flow in heterogeneous porous media. Figure 12b shows a significant difference between T_e calculated by TOUGH2 and T_e predicted by the prediction method. Furthermore, the predicted result exhibits disagreement with the decline rate of the calculated temperature for the case of spatially varying permeability of the surrounding rocks as well as the heat loss model (Gringarten and Sauty 1975). This is because both models consider the heat transfer solely due to advection and they are incapable of expressing gradual temperature change.

These comparisons imply that the fHTE can offer an accurate evaluation of temperature profiles and an elaborate characterization of thermal response in a fault-related subsidiary structure. As mentioned previously, the fADE can summarize complexity based on fractal geometry and can quickly and efficiently analyze mass transport in a fractured reservoir. In addition, our previous study has demonstrated that the fADE offers a method for predicting tracer responses irrespective of well intervals in a frac-

tured reservoir (Suzuki et al. 2012). Future developments from this study will include prediction of thermal breakthrough irrespective of well intervals and optimization of the well location and/or the condition of injection. The fHTE is expected to be a powerful tool for predicting premature thermal breakthrough in a fractured reservoir.

5 Conclusions

On the basis of the derivation of the fADE, a heat transfer model using fHTE was developed for the characterization of geothermal reservoirs. The effects of diffusion and heat transfer into a fault-related subsidiary structure were discussed. The interior of the reservoir is assumed to be uniform. The fADE and fHTE take into account fractal geometry, in which the diffusivity and heat conductivity vary with distance from the fault according to a power law.

A general reservoir simulator, TOUGH2, was used to generate reservoir performance data. It revealed the influence of different permeability patterns in the surrounding rocks. Conventional advection–dispersion models can describe tracer and thermal responses only for impermeable surrounding rocks. An increase in the permeability of the surrounding rocks leads to a long tail in the tracer response and a gradual temperature decline. The fADE solution was found to be in reasonable agreement with the tracer response for spatially varying permeability distributions, but the agreement with constant permeability was less satisfactory. Curve fittings on the temperature profile suggest that the fHTE can be used to interpret temperature profiles in fractured media. Higher permeability of the surrounding rocks resulted in an increase in the retardation parameters in the fADE and the fHTE. The fractional orders in the fADE and the fHTE may characterize the difference in the permeability patterns in the surrounding rocks. The fHTE provides an improvement over traditional methods for capturing the temperature decline.

Acknowledgments This work was supported by a Grant-in-Aid for the Japan Society for the Promotion of Science (Grant Number 23-3250).

References

Aksoy N, Serpen U, Filiz Ş (2008) Management of the Balcova–Narlidere geothermal reservoir, Turkey. Geothermics 37(4):444–466

Axelsson G, Flovenz OG, Hauksdottir S, Hjartarson A, Liu J (2001) Analysis of tracer test data and injection induced cooling in the Laugaland geothermal field, N-Iceland. Geothermics 30:697–725

Benson DA, Wheatcraft SW, Meerschaert MM (2000) Application of a fractional advection–dispersion equation. Water Resour Res 36(6):1403–1412

Bodvarsson GS (1972) Thermal problems in siting of reinjection wells. Geothermics 1(2):63–66

Bodvarsson GS, Tsang CF (1982) Injection and thermal breakthrough in fractured geothermal reservoirs. J Geophys Res 87(B2):1031–1048

Carslaw HS, Jaeger JC (1959) Conduction of heat in solids, 2nd edn. Oxford Science Publications, Oxford

Coats KD, Smith BD (1964) Dead-end pore volume and dispersion in porous media. Soc Pet Eng 4:73–84

Evans JP, Forster CB, Goddard JV (1997) Permeability of fault-related rocks, and implications for hydraulic structure of fault zones. J Struct Geol 19(11):1393–1404

Fomin SA, Chugunov VA, Hashida T (2005) The effect of non-Fickian diffusion into surrounding rocks on contaminant transport in a fractured porous aquifer. Proc R Soc A Math Phys Sci 461:2923–2939

Fomin SA, Chugunov VA, Hashida T (2011) Non-Fickian mass transport in fractured porous media. Adv Water Resour 34(2):205–214

Gringarten AC, Sauty JP (1975) A theoretical study of heat extraction from aquifers with uniform regional flow. J Geophys Res 80(35):4956–4962

Le Garzic E, de L'Hamaide T, Diraison M, Geraud Y, Sausse J, de Urreiztieta M, Hauville B, Champanhet J (2011) Scaling and geometric properties of extensional fracture systems in the proterozoic basement of Yemen. Tectonic interpretation and fluid flow implications. J Struct Geol 33(4):519–536

Horne RN (1981) Tracer analysis of fractured geothermal systems. GRC Trans 5:291–294

Huang Q, Huang G, Zhang H (2008) A finite element solution for the fractional advection–dispersion equation. Adv Water Res 31(12):1578–1589

Kocabas I (2004) Geothermal reservoir characterization via thermal injection backflow and interwell tracer testing. Geothermics 34(1):27–46

Lauwerier HA (1955) The transport of heat in an oil layer caused by the injection of hot fluid. Appl Sci Res 5(2–3):145–150

Massart B, Paillet M, Henrion V, Sausse J, Dezayes C, Genter A, Bisset A (2010) Fracture characterization and stochastic modeling of the granitic basement in the HDR Soultz project (France). Proc World Geotherm Congr 1:1–7

Pruess K, Oldenburg C, Moridis G (1999) TOUGH2 user's guide, version 2.0. LBL, Report, LBNL-43134

Samko SG, Kilbas AA, Marichev OI (1993) Fractional integrals and derivatives: theory and applications. Gordon and Breach, London

Savage H, Brodsky E (2011) Collateral damage: evolution with displacement of fracture distribution and secondary fault strands in fault damage zones. J Geophys Res 116(B3):B03405. doi:10.1029/2010JB007665

Shook GM (2001) Predicting thermal breakthrough in heterogeneous media from tracer tests. Geothermics 30(6):573–589

Suzuki A, Makita H, Niibori Y, Fomin SA, Chugunov VA, Hashida T (2012) Characterization of tracer responses using fractional derivative-based mathematical model and its application to prediction of mass transport in fractured reservoirs. GRC Trans 36:1391–1396

Welty J, Wicks CE, Rorrer GL, Wilson RE (2007) Fundamentals of momentum, heat and mass transfer, 5th edn. Wiley, New York

Woods AW, Fitzgerald SD (1993) The vaporization of a liquid front moving through a hot porous rock. J Fluid Mech 251:563–579

Xiao B, Yu B, Wang Z, Chen L (2009) A fractal model for heat transfer of nanofluids by convection in a pool. Phys Lett A 373(45):4178–4181

Zhang X, Lv M, Crawford JW, Young IM (2007) The impact of boundary on the fractional advection–dispersion equation for solute transport in soil: defining the fractional dispersive flux with the Caputo derivatives. Adv Water Resour 30(5):1205–1217